ORIGINAL ARTICLE

Targeting p16^{INK4a} Promotes Lipofibroblasts and Alveolar Regeneration after Early-Life Injury

Maéva Zysman[1], Bruno Ribeiro Baptista[1,2], Laure-Aléa Essari[1,2], Sara Taghizadeh[3], Charlotte Thibault de Ménonville[1], Clément Giffard[1], Amelle Issa[4], Marie-Laure Franco-Montoya[1], Marielle Breau[1], Rachid Souktani[1], Abdel Aissat[1], Laurence Caeymaex[5], Muriel Lizé[6], Jeanne Tran Van Nhieu[1,7], Camille Jung[4], Robert Rottier[8,9], Marcio Do Cruzeiro[10,11,12], Serge Adnot[1,13], Ralph Epaud[1,14], François Chabot[2], Sophie Lanone[1], Jorge Boczkowski[1]*, and Laurent Boyer[1,13]*

[1]Univ Paris Est Creteil, INSERM, IMRB, Creteil, France; [2]Service de Pneumologie, Centre Hospitalier Universitaire, Université de Lorraine, Vandœuvre-lès-Nancy, France; [3]Department of Pulmonary and Critical Care Medicine, Key Laboratory of Interventional Pulmonology of Zheijiang Province, First Affiliated Hospital of Wenzhou Medical University, Wenzhou, China; [4]Centre de Recherche Clinique, Centre de Ressource Biologique, Centre Hospitalier Intercommunal, Creteil, France; [5]Soins Intensifs Néonataux, Centre Hospitalier Intercommunal, Creteil, France; [6]Molecular and Experimental Pneumology Group, Clinic for Cardiology and Pneumology, University Medical Center Goettingen, Goettingen, Germany; [7]Service de Pathologie, Hôpital Henri Mondor, AP-HP, Hôpital Henri Mondor, Creteil, France; [8]Department of Pediatric Surgery, Erasmus Medical Center–Sophia Children's Hospital, Rotterdam, the Netherlands; [9]Department of Cell Biology, Erasmus Medical Center, Rotterdam, the Netherlands; [10]INSERM U1016, Institut Cochin, Paris, France; [11]UMR 8104, Centre National de la Recherche Scientifique, Paris, France; [12]Université Paris Descartes, Sorbonne, Paris, France; [13]Service de Physiologie, Hôpital Henri Mondor, AP-HP, Creteil, France; and [14]Service de Pédiatrie, Centre des Maladies Respiratoire Rares, Centre Hospitalier Intercommunal, Creteil, France

ORCID IDs: 0000-0003-3830-1039 (R.E.); 0000-0003-2509-8799 (S.L.); 0000-0002-2608-6696 (L.B.).

Abstract

Rationale: Promoting endogenous pulmonary regeneration is crucial after damage to restore normal lungs and prevent the onset of chronic adult lung diseases.

Objectives: To investigate whether the cell-cycle inhibitor p16^{INK4a} limits lung regeneration after newborn bronchopulmonary dysplasia (BPD), a condition characterized by the arrest of alveolar development, leading to adult sequelae.

Methods: We exposed p16$^{INK4a-/-}$ and p16^{INK4a} *ATTAC* (apoptosis through targeted activation of caspase 8) transgenic mice to postnatal hyperoxia, followed by pneumonectomy of the p16$^{INK4a-/-}$ mice. We measured p16^{INK4a} in blood mononuclear cells of preterm newborns, 7- to 15-year-old survivors of BPD, and the lungs of patients with BPD.

Measurements and Main Results: p16^{INK4a} concentrations increased in lung fibroblasts after hyperoxia-induced BPD in mice and persisted into adulthood. p16^{INK4a} deficiency did not protect against hyperoxic lesions in newborn pups but promoted restoration of the lung architecture by adulthood. Curative clearance of p16^{INK4a}-positive cells once hyperoxic lung lesions were established restored normal lungs by adulthood. p16^{INK4a} deficiency increased neutral lipid synthesis and promoted lipofibroblast and alveolar type 2 (AT2) cell development within the stem-cell niche. Besides, lipofibroblasts support self-renewal of AT2 cells into alveolospheres. Induction with a PPARγ (peroxisome proliferator–activated receptor γ) agonist after hyperoxia also increased lipofibroblast and AT2 cell numbers and restored alveolar architecture in hyperoxia-exposed mice. After pneumonectomy, p16^{INK4a} deficiency again led to an increase in lipofibroblast and AT2 cell numbers in the contralateral lung. Finally, we observed p16^{INK4a} mRNA overexpression in the blood and lungs of preterm newborns, which persisted in the blood of older survivors of BPD.

Conclusions: These data demonstrate the potential of targeting p16^{INK4a} and promoting lipofibroblast development to stimulate alveolar regeneration from childhood to adulthood.

Keywords: alveolar regeneration; adult consequences of bronchopulmonary dysplasia; p16^{INK4a} lipofibroblasts

(Received in original form August 12, 2019; accepted in final form July 1, 2020)

*These authors contributed equally to this work.

Correspondence and requests for reprints should be addressed to Laurent Boyer, M.D., Ph.D., Institut Mondor de Recherche Biomédicale, Université Paris–Est, 8 Rue du Général Sarrail, 94000 Créteil, France. E-mail: laurent.boyer@aphp.fr.

This article has a related editorial.

This article has an online supplement, which is accessible from this issue's table of contents at www.atsjournals.org.

Am J Respir Crit Care Med Vol 202, Iss 8, pp 1088–1104, Oct 15, 2020

Originally Published in Press as DOI: 10.1164/rccm.201908-1573OC on July 6, 2020
Internet address: www.atsjournals.org

At a Glance Commentary

Scientific Knowledge on the Subject: Lung regeneration is critical for recovering after lung damage. However, several lung diseases, such as bronchopulmonary dysplasia, are associated with lifelong lung sequelae in survivors without an efficient endogenous lung regeneration. The induction of cell-cycle inhibitors during disease may limit this process. Among them, the protein $p16^{INK4a}$ is of specific interest, as it contributes to the age-associated decline of pancreatic islet, bone marrow, and neural tissues.

What This Study Adds to the Field: This study identifies a beneficial role for targeting $p16^{INK4a}$ deficiency to promote lung regeneration after bronchopulmonary dysplasia. This effect is mediated by lipofibroblast differentiation in the stem cell niche, which enables promotion of new alveolar formation after hyperoxic injury. This could be a new, interesting pathway to induce catch-up growth between early-life injury and adulthood.

Lung regeneration is critical for recovering after lung damage or to protect against age-associated decline. Thus, promoting endogenous regeneration through stem cells to restore lung architecture and function may be promising for the future therapy of respiratory diseases (1–3). However, clinical trials targeting endogenous regeneration have failed to improve the onset of chronic lung diseases (4, 5). This highlights the need to better understand the molecular mechanisms that limit the regeneration of lungs damaged because of lung disease.

The induction of cell-cycle inhibitors during disease processes may limit lung regeneration. Among them, the protein $p16^{INK4a}$, encoded by the *CDKN2A* (cyclin-dependent kinase inhibitor 2A) locus, is of specific interest, as it contributes to the age-associated decline of pancreatic islet, bone marrow, and neural tissues (6–12). Although $p16^{INK4a}$ accumulates in the lungs with age, whether this protein disturbs their capacity to regenerate is yet to be determined.

We hypothesized that targeting $p16^{INK4a}$ could enhance lung regeneration after injury. We addressed this hypothesis using bronchopulmonary dysplasia (BPD) as a model. BPD is a common complication of prematurity, characterized by developmental arrest of the lungs, with impaired alveolar septation. These alterations lead to lifelong sequelae in survivors, such as the alteration of lung function (13–18). No therapeutic intervention is currently available for survivors of BPD to restore normal lung function in adulthood (19).

We assessed whether $p16^{INK4a}$ plays a causative role in limiting lung regeneration using an experimental mouse model of BPD induced by neonatal exposure to hyperoxia associated with morphological, physiological, and molecular analyses of the lung and pharmacological interventions in both $p16^{INK4a-/-}$ and $p16^{INK4a}$ *ATTAC* (apoptosis through targeted activation of caspase 8) mice (11). These experiments demonstrated a critical role for $p16^{INK4a}$ deficiency in promoting lung regeneration after hyperoxia-induced arrest of alveolarization. This process was mediated by lipofibroblast differentiation in the stem cell niche. In addition, the induction of differentiation after hyperoxia with a PPARγ (peroxisome proliferator–activated receptor γ) agonist restored alveolar architecture. These results were confirmed in a pneumonectomy model, leading to compensatory realveolarization of the remaining lung. Finally, $p16^{INK4a}$ expression was higher in the cord blood cells from preterm newborns than that from full-term control animals. This was associated with the induction of $p16^{INK4a}$ in the lungs of patients with BPD. Furthermore, elevated $p16^{INK4a}$ concentrations in blood cells persisted in 7- to 15-year-old survivors of BPD. Thus, targeting $p16^{INK4a}$ could become an innovative therapeutic strategy to promote alveolar regeneration.

Some of the results of these studies have been previously reported in the form of abstracts from European Respiratory Society congresses in 2017, 2018, and 2019 (20–22).

Methods

For additional details on the methods, *see* the online supplement.

Animals

Animal use was approved by the French Institutional Animal Care Committee. $p16^{INK4a-/-}$ mice were provided by A. Bern (23), and *ATTAC* mice were provided by S. Adnot for inducible elimination of $p16^{INK4a}$-positive cells (11).

Hyperoxic Exposure

Mouse pups were exposed to an 85% (hyperoxia) or 21% (room air or normoxia) $F_{I_{O_2}}$ from Day 3 (D3) to D14 (Figure 1A) (24, 25).

Drug Administration

We injected rosiglitazone or T0901317 (Bertin) from D14 to D60.

Pneumonectomy Procedure

We performed left-lung removal as described (26).

Morphometry

Standard morphometric methods were used (mean linear intercept [MLI]) (27), and immunostaining was performed according to standard procedures.

Microarray Analyses

The Mouse Gene 2.0 microarray (Affymetrix) was used at D14 and D60.

Real-Time PCR

Analyses were performed, and gene expression was presented as that relative to the expression of the housekeeping gene Hprt1 (hypoxanthine-guanine

Supported by a fellowship from la Fondation pour la Recherche Médicale (M.Z.; bourse Marianne Josso, Paris, France); Lorraine University, Nancy, France (B.R.B. and L.-A.E.); and grants from Novartis (M.Z. and C.G.), Oxyvie (C.G.), and ARAIRLOR (M.Z.).

Author Contributions: M.Z., J.B., and L.B. conceived and designed the study. M.Z., B.R.B., L.-A.E., S.T., C.T.d.M., C.G., A.I., M.-L.F.-M., M.B., L.C., and R.S. performed experiments. M.Z., B.R.B., L.-A.E., and A.A. analyzed gene-expression and human-expression data. M.L., J.T.V.N., C.J., M.D.C., S.A., R.E., F.C., and S.L. provided critical analysis and discussions. R.R. provided bronchopulmonary dysplasia lung samples. M.Z., J.B., and L.B. wrote the paper with significant input and contributions. All coauthors reviewed and approved the final manuscript.

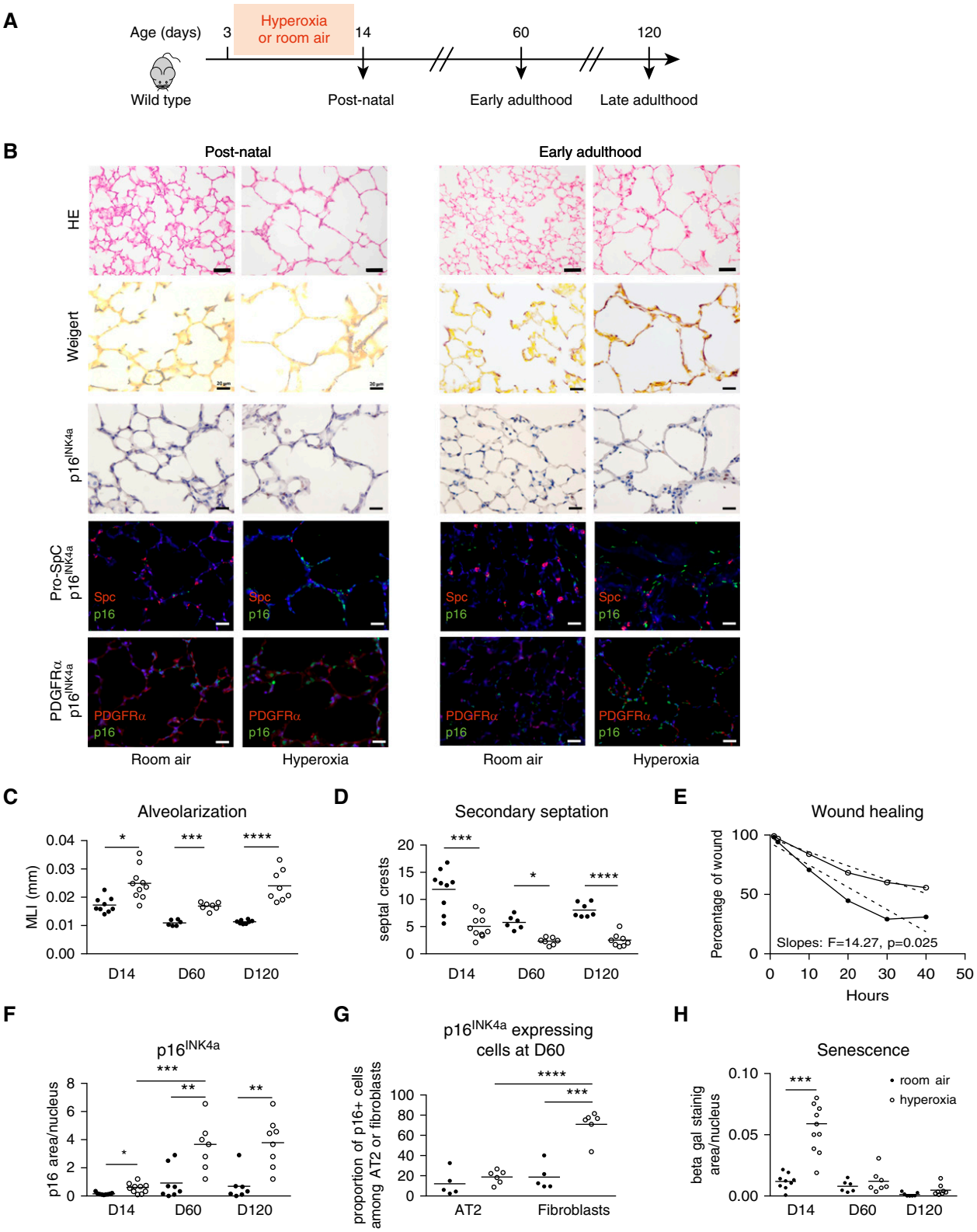

Figure 1. Exposure of immature mouse lungs to hyperoxia engenders sequelae at adulthood. p16^{INK4a} concentrations in fibroblasts increase early, and this induction is amplified in adulthood and is associated with cell senescence. (*A*) Timeline of exposure to hyperoxia. Mice were exposed to hyperoxia, versus room air, from Day 3 (D3) to D14 and were then exposed to room air. Lungs were harvested at D14, D60, and D120. (*B*) HE staining, elastin staining by the Weigert technique, immunostaining of p16^{INK4a}, immunofluorescence of Pro-SftpC and p16^{INK4a}, and immunofluorescence of PDGFRα (platelet-derived growth factor α) and p16^{INK4a}. (*C*) Quantification of the mean linear intercept. (*D*) Septal crest counts. (*E*) Speed of wound healing, after scratch

phosphoribosyl transferase 1) (*see* Table E1 in the online supplement).

Lipidomics Analyses

Lipids were extracted from whole lung at D60, as previously described (28).

Cell Culture

Primary fibroblasts were isolated from mouse lungs.

Alveolospheres

The total alveolar type 2 (AT2) cell population ($Sftpc^{+}Tom^{high}$ [$Sftpc^{+}$ and translocase of the outer mitochondrial membrane–high] cells) was isolated from lungs of 6- to 8-week-old $Sftpc^{CreERT2/+}$; $tdTomato^{flox/flox}$ (phenotype with Cre recombinase fused to a mutant estrogen ligand–binding domain *Sftpc* allele variant/wild-type *Sftpc* allele variant; floxed tandem-dimer Tomato) mice. For the isolation of mesenchymal cells of interest, we first sorted an enriched population of $Cd45^{-}Cd31^{-}Epcam^{-}Sca1^{+}$ ($Cd45^{-}$, $Cd31^{-}$, epithelial cell adhesion molecule–negative, and spinocerebellar ataxia type 1–positive) cells. $LipidTOX^{+}$ and $LipidTOX^{-}$ cells were isolated from the $Sca1^{+}$ population. For the isolation of epithelial cells from the $Sftpc^{CreERT2/+}$; $tdTomato^{flox/flox}$ lungs, we first sorted a population of $Cd45^{-}Cd31^{-}Epcam^{+}$ cells, enriched with mature AT2 cells, using Lysotracker (no. L7526; Invitrogen). Fluorescence-activated sorted cells were resuspended in media and mixed 1:1 with growth factor–reduced phenol Red-free Matrigel (no. 356231; Corning). Spheres were counted and measured at D14.

Human Blood Samples

We measured $p16^{INK4a}$ expression in peripheral blood mononuclear cells from cord blood of very preterm newborns (<24 wk of gestational age), matched with full-term newborns, and in peripheral blood mononuclear cells from survivors of BPD who were 7–15 years of age, matched with full-term children (Centre Hospitalier Intercommunal Créteil, unpublished results; clinicaltrials.gov identifier NCT 03540680).

Human Lung Samples

Lung sections from patients with BPD were provided by Dr. R. Rottier (29).

Statistical Analysis

GraphPad Prism 6 was used for all statistical analysis. The Student's *t* test (unpaired, two-tailed) and two-way ANOVA were used appropriately. Data are presented as the mean ± SEM, and differences were considered to be statistically significant if *P* values were less than 0.05.

Results

Exposure of Immature Mouse Lungs to Hyperoxia Results in Sequelae and Elevated $p16^{INK4a}$ Expression in Adulthood

Exposure of newborn C57BL/6J mice to 85% O_2 during the alveolarization period, from D3 to D14 of postnatal life (Figure 1A) radically arrested alveolar development, reducing the number of alveoli (MLI), with a concomitant disruption of secondary septation, relative to that of mice exposed to room air (Figures 1A–1D and E1A–E1E).This had long-term consequences, revealed by the persistence of a higher MLI and lower secondary septation at early and late adulthood (D60 and D120, respectively) in mice exposed to hyperoxia compared with those exposed to room air (Figures 1B and 1D). Lung fibroblasts, which are essential for secondary septation during alveologenesis, isolated from 14-day-old hyperoxic pups had a significantly lower wound-healing velocity than those of normoxic animals (Figures 1E and E3). Lung function was also altered, with a decrease in dynamic lung elastance and exercise capacity at D60 in mice exposed to hyperoxia (Figures 2E and 2H).

The proportion of cells expressing $p16^{INK4a}$ in the alveolar wall increased four times immediately after hyperoxia relative to normoxia (D14, Figures 1B and 1F) (30). This phenomenon was amplified at early and late adulthood (Figures 1B and 1F). Costaining of $p16^{INK4a}$ and PDGFRα (platelet-derived growth factor α) or pro-SpC (for fibroblasts and AT2 cells respectively) showed that ∼20% of fibroblasts and AT2 cells expressed $p16^{INK4a}$ in normoxic mice at D14. This percentage remained similar for AT2 cells in hyperoxic mice but reached more than 70% in fibroblasts (Figure 1G). Thus, $p16^{INK4a}$ was significantly induced in mesenchymal cells after hyperoxia. $p16^{INK4a}$ overexpression was associated with an induction of cell senescence in the lungs at D14 (31, 32), but this difference disappeared by adulthood (D60 and D120; Figures 1H and E1B) (33). We obtained similar results for p21 mRNA expression in whole-lung homogenates (data not shown).

Overall, exposure of mouse lungs to hyperoxia results in arrested alveolarization, with sequelae at adulthood associated with $p16^{INK4a}$ overexpression in lung fibroblasts.

$p16^{INK4a}$ Deficiency Does Not Protect against Early Hyperoxia–induced Hypoalveolarization but Restores Normal Lung Architecture at Adulthood

Hyperoxia induced $p16^{INK4a}$ expression, which was amplified at adulthood. We thus assessed the structure of the lungs of wild-type and $p16^{INK4a-/-}$ mice from D14 to 120. The lungs of normoxic $p16^{INK4a-/-}$ and wild-type lungs were similar in terms of MLI and septal crests at each time point (Figures 2B–2D and E1D and E1E). Immediately after hyperoxia (D14), there was no difference between the lungs of $p16^{INK4a-/-}$ and wild-type mice (Figures 2B–2D), showing that $p16^{INK4a}$ deficiency did not protect against hyperoxia-induced hypoalveolarization.

Two days after the end of hyperoxia (D16), $p16^{INK4a}$ deficiency was associated with a modest but significant increase in the number of septal crests relative to that of wild-type mice (Figures E1C and E1E). This early sign of a protective effect of $p16^{INK4a}$ deletion was confirmed at early and late adulthood (D60 and D120, respectively, Figures 2B and 2G and E1E). The MLI

Figure 1. (*Continued*). test. (*F*) Quantification of the area of $p16^{INK4a}$ staining/nuclear staining. (*G*) Proportion of p16-positive cells among AT2 cells or fibroblasts at D60. (*H*) Quantification of the area of senescence-associated β-galactosidase staining/nuclear staining. Solid circles indicate room air; open circles indicate hyperoxia. Scale bars, 20 μm. $^{*}P < 0.05$, $^{**}P < 0.01$, $^{***}P < 0.001$, and $^{****}P < 0.0001$. AT2 = alveolar type 2; HE = hematoxylin and eosin; MLI = mean linear intercept.

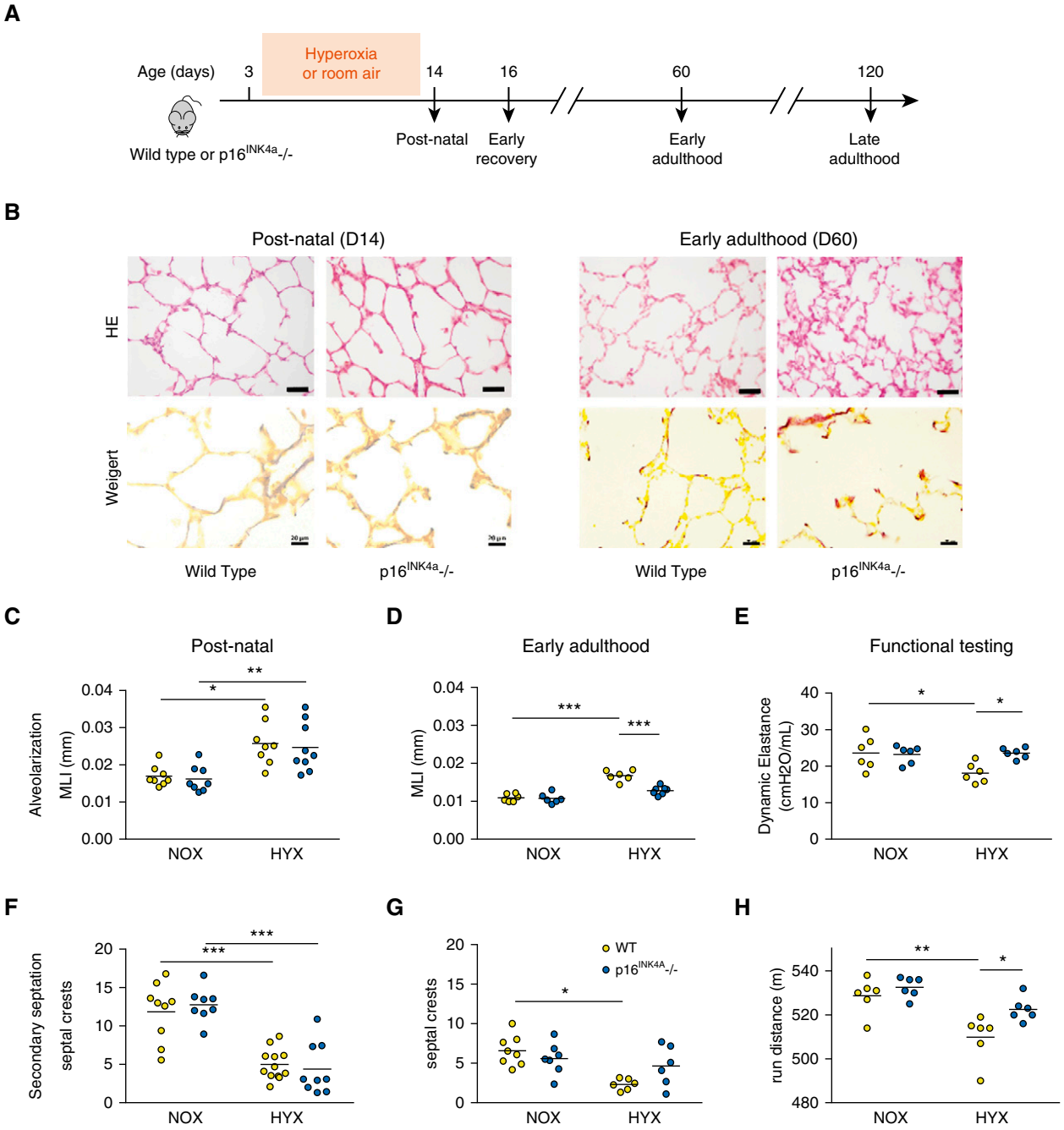

Figure 2. p16^{INK4a} deficiency does not protect against hyperoxia-induced hypoalveolarization but restores normal lung architecture by adulthood in mice exposed to postnatal hyperoxia. (*A*) Timeline of exposure to hyperoxia. Wild-type (WT) and p16$^{INK4a-/-}$ mice were exposed to hyperoxia, versus room air, from Day 3 (D3) to D14 and then exposed to room air. Lungs were harvested at D14, D16, D60, and D120. (*B*) HE staining and elastin staining by the Weigert technique. (*C* and *D*) Quantification of the mean linear intercept at D14 and D60. (*E*) Functional testing; dynamic elastance. (*F* and *G*) Septal crest counts at D14 and D120. (*H*) Run distance. Yellow circles indicate WT; blue circles indicate p16$^{INK4a-/-}$. Scale bars, 20 μm. $^{*}P < 0.05$, $^{**}P < 0.01$, and $^{***}P < 0.001$. HE = hematoxylin and eosin; HYX = hyperoxic mice; MLI = mean linear intercept; NOX = normoxic mice.

decreased by 30% at D60 and by 71% at D120 in p16^{INK4a}-deficient mice relative to wild-type mice, reaching the same amount as those of both wild-type and p16^{INK4a}-deficient room-air mice (Figures 2C and E1E).

At D120, p16^{INK4a} deficiency normalized elastance and improved exercise capacity (+12% running distance, Figures 2E and 2H). In summary, p16^{INK4a} deficiency restored lung architecture and function in adult mice exposed to neonatal hyperoxia. This process was dynamic, starting early after the cessation hyperoxia but still continuing at a time distant from that of the initial damage.

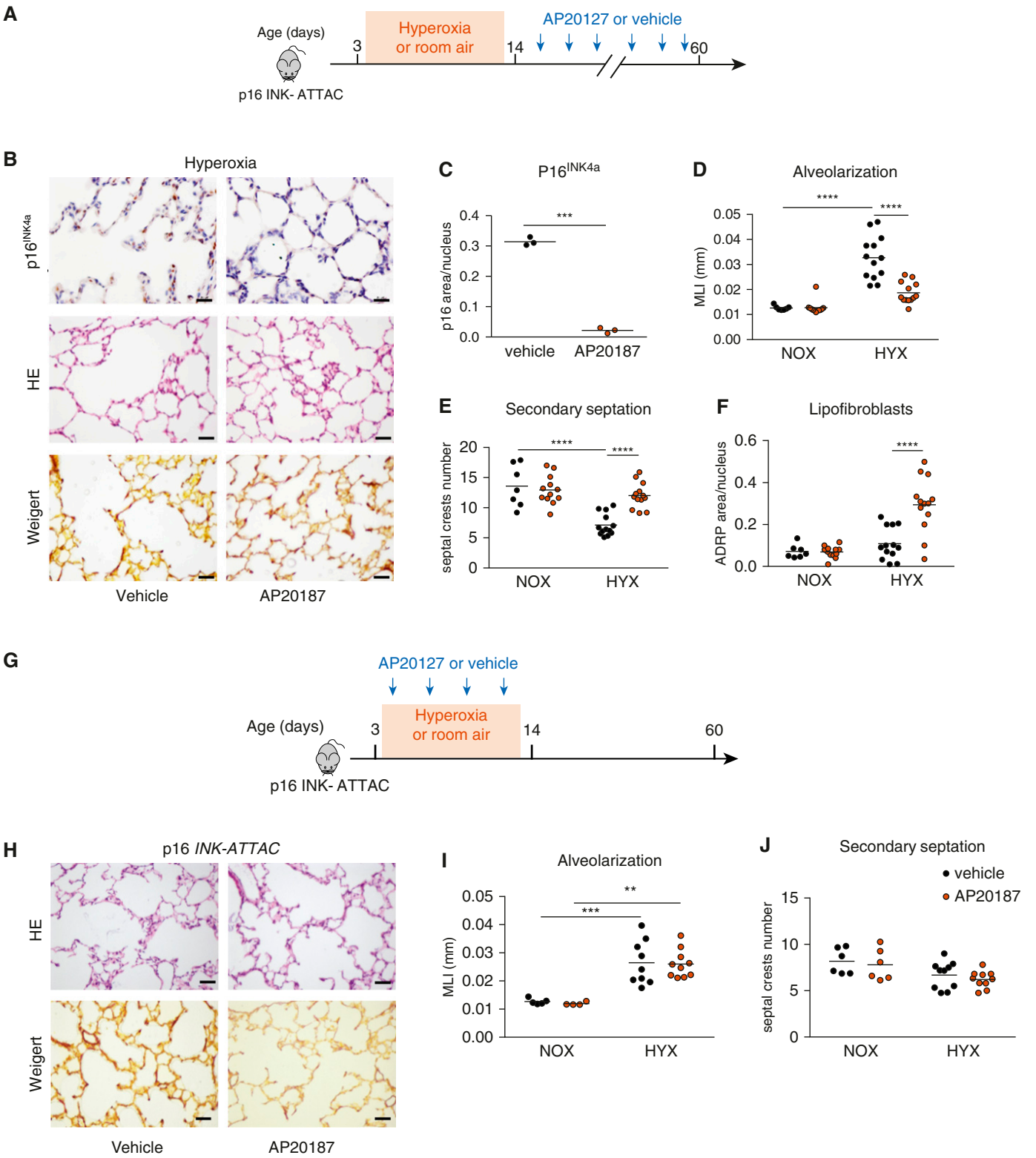

Figure 3. Clearance of p16^{INK4a}-expressing cells restores the lung architecture by adulthood after early-life exposure to hyperoxia. (*A*) Timeline of exposure to hyperoxia. p16 *ATTAC* (apoptosis through targeted activation of caspase 8) mice were exposed to hyperoxia, versus room air, from Day 3 (D3) to D14 and then were exposed to room air. One group was treated with AP20187 and another was treated with vehicle from D15 to D60. Lungs were harvested at D60. (*B*) Immunostaining of p16^{INK4a} showing that clearance of p16^{INK4a}-expressing cells is efficient at D20; HE staining and elastin staining by the Weigert technique in early adulthood (D60). (*C*) Quantification of p16^{INK4a}. (*D*) Quantification of the mean linear intercept in early adulthood (D60). (*E*) Septal crest counts in early adulthood (D60). (*F*) ADRP (adipose differentiation–related protein) staining in early adulthood (D60). (*G*) Timeline of exposure to

We evaluated collagen deposition (Sirius Red, collagen 1 and 3 immunostaining) to determine whether lung restoration was associated with fibrosis (1, 34) or whether it was due to true lung regeneration. Collagen deposition was not modulated in hyperoxic wild-type mice at any time point. Septal thickness and collagen deposition, especially that of collagen 1, was greater in the alveolar walls of hyperoxic $p16^{INK4a-/-}$ mice than in wild-type mice at D60, but this difference disappeared by D120 (Figure E5). Thus, $p16^{INK4a}$ deficiency was associated with an ongoing process of lung regeneration after early hyperoxia that led to successful *de novo* alveolarization.

Clearance of $p16^{INK4a+}$ Cells Restores Normal Lungs at Adulthood

We demonstrated that $p16^{INK4a}$ deficiency restores normal lungs at adulthood in mice exposed to early-life hyperoxia. We thus examined whether eliminating $p16^{INK4a+}$ cells once lesions were established could also restore normal lungs. We used *INK* (inhibitor of cyclin-dependent kinase)–*ATTAC* transgenic mice (12) to induce apoptosis in $p16^{INK4a+}$ cells, starting just after hyperoxia exposure (D14) and continuing to adulthood (D60; Figure 3A) (12). $p16^{INK4a}$ *ATTAC* had no specific phenotype in mice exposed to room air. Hyperoxia dramatically altered alveolar development at D14, and this effect lasted until D60 among $p16^{INK4a}$ *ATTAC* mice treated with vehicle (Figures 3C–3E). However, $p16^{INK4a+}$ cell clearance efficiently restored lung architecture, with the normalization of MLI and the number of septal crests by D60 (Figures 3B–3E), whereas treating mice concurrently with hyperoxia (Figures 3G) to block the initial trigger did not modify $p16^{INK4a}$ expression at D60 and was insufficient to restore normal lung architecture (Figures 3H–3J), suggesting that regular clearance of $p16^{INK4a}$ after hyperoxia is essential to lung regeneration.

$p16^{INK4a}$ Deletion Confers a Lipogenic Switch during Resolution at Adulthood after Murine Hyperoxic-Injury Model

We performed microarray analyses on whole-lung homogenates after hyperoxia (D14) and at D60 to further understand the mechanisms of the regenerative process triggered by $p16^{INK4a}$ suppression. The number of genes modulated by $p16^{INK4a}$ deficiency in hyperoxic mice increased from 219 at D14 to 612 at D60 (Figure 4B). Only 14 genes modulated by $p16^{INK4a}$ deficiency were common between D14 and D60, suggesting a dynamic transcriptional process. We mainly observed increased expression of genes associated with lipogenesis pathways in $p16^{INK4a-/-}$ mice exposed to hyperoxia relative to wild-type mice at adulthood (Figure 4A), such as Srebp1 (sterol regulatory element–binding protein 1) and Srebp2, Insig1 (insulin-induced gene 1) and Insig2, and Scap (SREBP cleavage-activating protein) (Figure 4A). Neither pathways associated with lung development, such as the FGF7 (fibroblast growth factor 7) pathway, nor senescence were modulated by $p16^{INK4a}$ deficiency (Figure E6).

We confirmed that hyperoxia reduced Srebp2, Scap, and Adrp (adipose differentiation–related protein) expression in both wild-type and $p16^{INK4a-/-}$ mice at D14 by quantitative PCR (Figures 4D and 4E). At D60, hyperoxia alone did not induce Srebp2 or Scap expression, but when associated with $p16^{INK4a}$ deficiency, Srebp2, Scap, and Adrp expression increased (Figure 4D).

We performed lipidomic analyses on whole lung at D60 to determine whether the activation of lipogenesis increased lipid content. Hyperoxia did not modulate the lipid composition in wild-type mice, whereas neutral lipids were differentially expressed in $p16^{INK4a-/-}$ mice: the concentration of 19 triacylglycerides increased (among 24), and 20 phospholipids or sphingolipids increased and 11 decreased (among 167; Figure 4C).

Overall, these results confirm the activation of lipogenesis pathways, increasing lipid synthesis, mainly neutral lipids, in the lungs because of $p16^{INK4a}$ deficiency.

$p16^{INK4a}$ Deficiency Promotes Lipogenic Fibroblast Differentiation and the Stem Cell Niche

Neutral lipids in the alveoli are primarily localized as lipid droplets in lipofibroblasts, interstitial fibroblasts involved in alveolar maturation and surfactant production during lung development (35–38). Lipid droplets consist of a neutral lipid core, mainly composed of triglycerides, essential for cellular metabolism and membrane production. We explored whether lipofibroblasts were involved in lung regeneration of $p16^{INK4a-/-}$ hyperoxic mice by analyzing isolated lung fibroblasts *in vitro* (Figure 5A). $p16^{INK4a-/-}$ fibroblasts showed augmented lipid-droplet content (Figure 5B) and upregulation of lipogenic genes relative to those of wild-type mice (Figure 5C). $p16^{INK4a}$ deficiency provided a better migratory phenotype to fibroblasts, as wound closure was accelerated (Figures 5D and E7).

We observed more lipid droplets in $p16^{INK4a-/-}$ hyperoxic lungs than in wild-type hyperoxic lungs at D60 *in vitro* (Figures 5E and 5F). We confirmed the presence of lipofibroblasts by measuring ADRP expression surrounding the lipid droplets (39). Hyperoxia initially markedly reduced ADRP expression, both in wild-type and $p16^{INK4a-/-}$ mice. On the second day after removing hyperoxia (D16), ADRP concentrations were similar between hyperoxic and normoxic wild-type mice, but hyperoxia-induced ADRP expression in $p16^{INK4a-/-}$ mice persisted until D120 (Figures 5H and E2A). Similarly, the clearance of $p16^{INK4a+}$ cells after hyperoxia was also associated with the increase of lipofibroblasts (Figure 3F). We further confirmed that $p16^{INK4a}$ deficiency resulted in an increase in the number of lipofibroblasts by fluorescence-activated cell sorting ($CD45^{-}CD31^{-}Epcam^{-}ADRP$

Figure 3. (*Continued*). hyperoxia. p16 *ATTAC* mice were exposed to hyperoxia, versus room air, from D3 to D14 and then were exposed to room air. One group was treated with AP20187 and another was treated with vehicle during hyperoxia from D3 to D15. Lungs were harvested in early adulthood (D60). (*H*) HE staining and elastin staining by the Weigert technique in early adulthood (D60). (*I*) Quantification of the mean linear intercept in early adulthood (D60). (*J*) Septal crest counts in early adulthood (D60). Black circles indicate vehicle; pink circles indicate AP20187. Scale bars, 20 μm. $^{**}P < 0.01$, $^{***}P < 0.001$, and $^{****}P < 0.0001$. HE = hematoxylin and eosin; HYX = hyperoxic mice; MLI = mean linear intercept; NOX = normoxic mice.

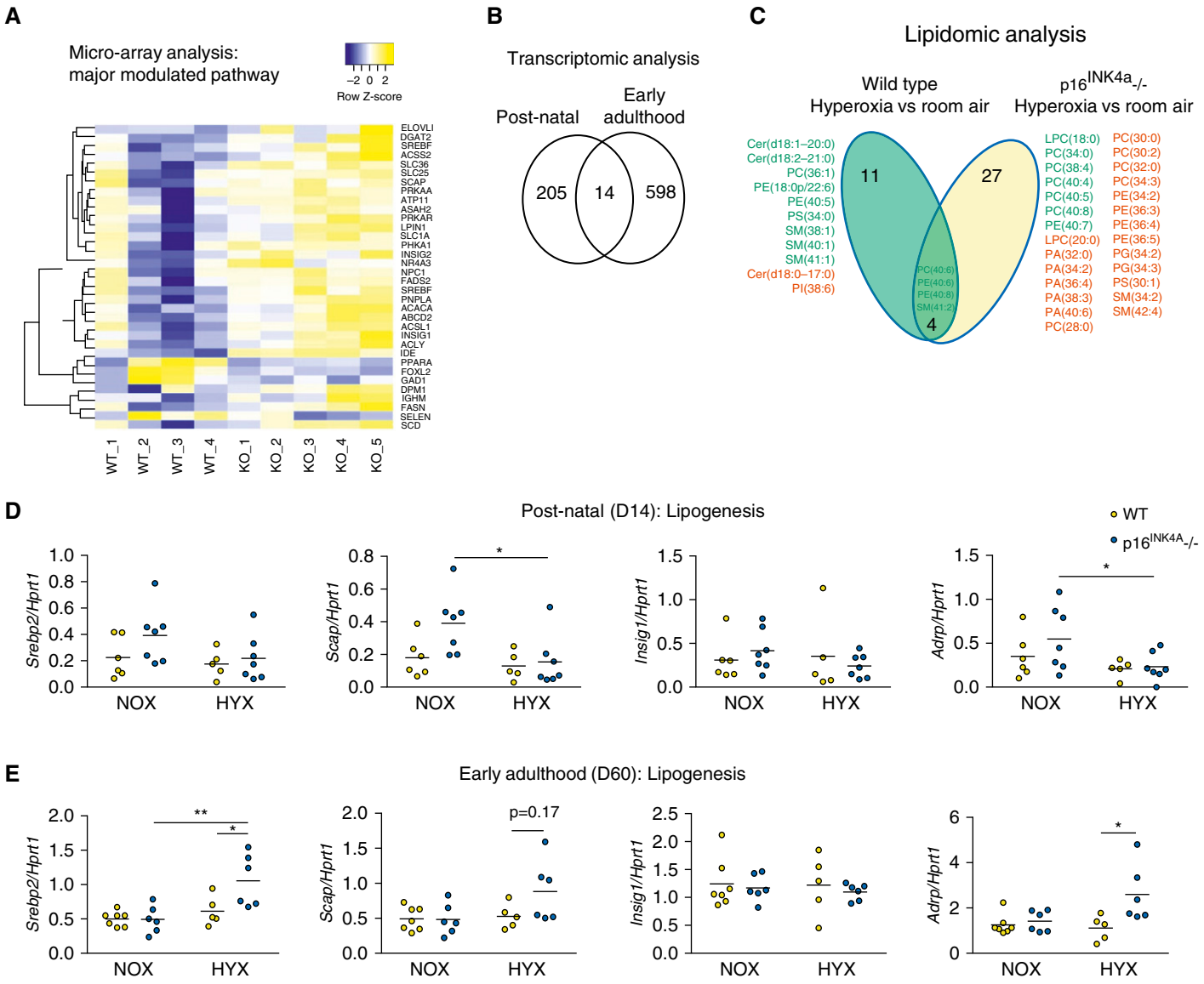

Figure 4. p16^{INK4a} deletion confers a lipogenic switch during the resolution of bronchopulmonary dysplasia in adulthood. (*A*) Microarray analysis of whole-lung homogenates, showing the main modulated pathway: activation of the lipogenesis pathways in p16$^{INK4a-/-}$ compared with wild-type (WT) hyperoxic mice. Yellow indicates upregulation; blue indicates downregulation. (*B*) Venn diagram of genes modulated at Days 14 (D14) and D60. (*C*) Lipidomic analysis of whole lung. Red indicates upregulation; green indicates downregulation. (*D*) Gene expression by quantitative PCR (qPCR): *Srebp2* (sterol regulatory element–binding protein 2), *Scap* (SREBP cleavage-activating protein), *Insig1* (insulin-induced gene 1), and *Adrp* (adipose differentiation–related protein) expression relative to that of the housekeeping gene *Hprt1* (hypoxanthine-guanine phosphoribosyl transferase 1) at D14. (*E*) Gene expression by qPCR: *Srebp2*, *Scap*, *Insig1*, and *Adrp* expression relative to that of the housekeeping gene *Hprt1* at D60. Yellow circles indicate WT; blue circles indicate p16$^{INK4a-/-}$. *$P < 0.05$ and **$P < 0.01$. HYX = hyperoxic mice; NOX = normoxic mice.

and/or LipidTOX$^+$) at D60 after hyperoxia (Figure 5K). In addition, CD45$^-$CD31$^-$Epcam$^-$PDGFRα$^+$, LipidTOX$^+$, and/or ADRP were increased (Figures 5K and E2C).

Given the ability of lipofibroblasts to differentiate into myofibroblasts during repair and promote fibrosis (36, 40), we tested whether p16^{INK4a} deficiency increased myofibroblast content. There was no difference between the groups at the various time points in terms of α-SMA expression, except transiently at D16 (Figure E5), thus excluding a fibrosis-driven process. Secondary crest myofibroblasts (also known as alveolar myofibroblasts) are initially PDGFRα$^+$ and later become α-SMA$^+$ and are found localized at the tip of the alveolar septa close to elastin (41). Using costaining of α-SMA and PDGFRα, we confirmed that alveolar myofibroblasts increased in septal crests from hyperoxia-exposed p16$^{INK4a-/-}$ mice compared with all other groups at D14 (Figure E2E). No difference was observed between groups at D60 (data not shown).

Altogether, p16^{INK4a} deficiency was associated with lipogenic differentiation of fibroblasts in the stem cell niche after hyperoxia.

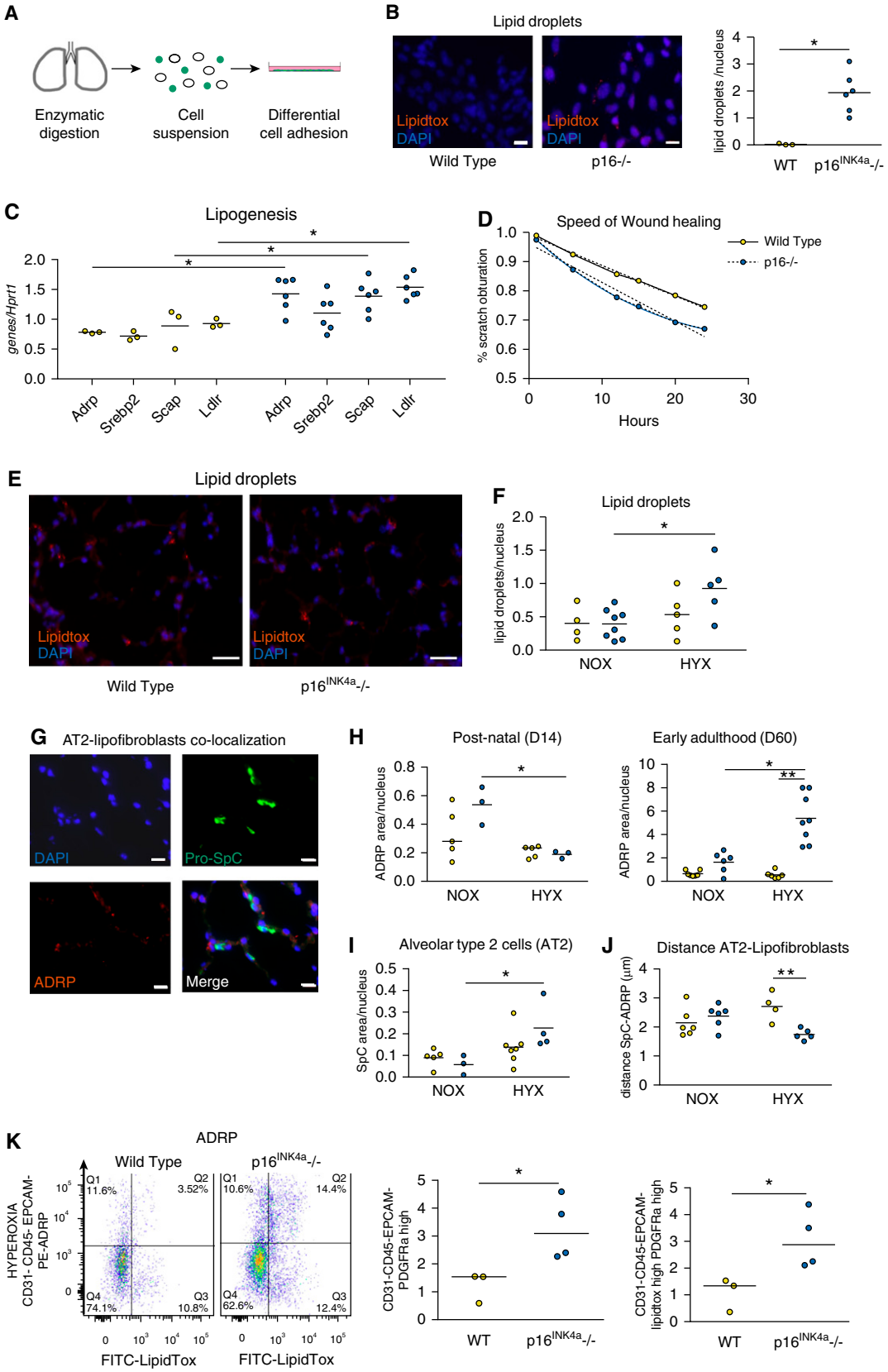

Figure 5. p16^{INK4a} deficiency promotes lipogenic fibroblast differentiation and development of the stem cell niche. (*A*) Isolation of fibroblasts from the lung by enzymatic digestion. (*B*) Lipid-droplet staining by LipidTOX Deep-Red staining and lipid-droplet counts. (*C*) Gene expression by quantitative PCR of the lipid-pathway genes *Adrp* (adipose differentiation–related protein), *Srebp2* (sterol regulatory element–binding protein 2), *Scap* (SREBP cleavage-activating

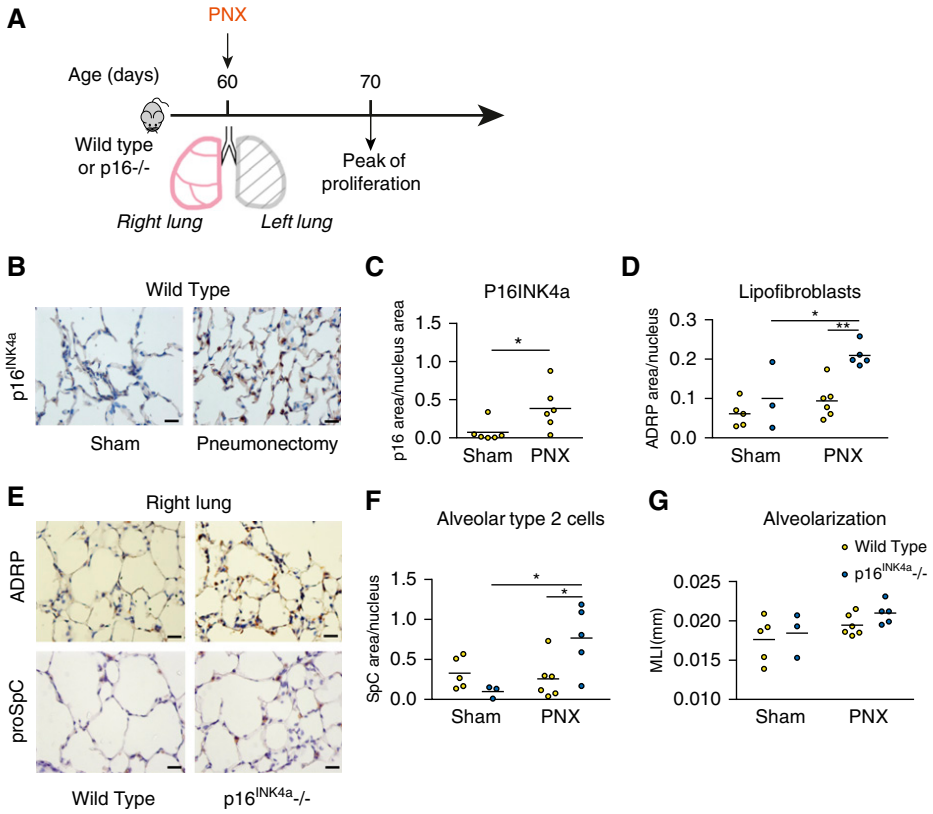

Figure 6. The lipogenic switch of fibroblasts can induce lung regeneration after pneumonectomy (PNX). $p16^{INK4a}$ deletion induces an increase in the number of lipofibroblasts (ADRP [adipose differentiation–related protein]-positive cells) and alveolar type 2 cells (pro-SpC–positive cells) in the lungs relative to control animals. (*A*) Timeline after PNX. Wild-type mice underwent either a left PNX or only a left thoracotomy. Lungs were harvested 10 days later. (*B*) Immunostaining of $p16^{INK4a}$ and (*C*) quantification of $p16^{INK4a}$ staining in wild-type mice: sham versus PNX. (*D*) Quantification of the area of ADRP staining/nuclear staining. (*E*) Immunostaining of ADRP, Pro-SpC, and arginase 1. (*F*) Quantification of the area of pro-Spc staining/nuclear staining. (*G*) MLIs. Yellow circles indicate wild type; blue circles indicate $p16^{INK4a-/-}$. Scale bars, 20 μm. $^{*}P < 0.05$ and $^{**}P < 0.01$. MLI = mean linear intercept.

Lipofibroblasts belong to the alveolar stem cell niche and are found next to AT2 cells (36, 42) to boost AT2-cell self-renewal and differentiation (42). We also confirmed that lipofibroblasts were adjacent to AT2 cells (Figure 5G). We further evaluated how lipofibroblasts formed the alveolar niche with AT2 cells by measuring the distance between the two types of cells using AT2 cells as an anchor point (43). The mean distance between lipofibroblasts and AT2 cells was smaller in the lungs of hyperoxic $p16^{INK4a-/-}$ mice than in those of all other groups, and the number of lipofibroblasts close to AT2 cells was higher in the lungs of $p16^{INK4a-/-}$ mice exposed to hyperoxia than in those of wild-type mice (Figure 5J). Finally, the number of AT2 cells was higher in the lungs of hyperoxic $p16^{INK4a-/-}$ mice than in the lungs of hyperoxic wild-type mice at D120 (Figures 5I and E2B). In addition, we observed lipid droplets in the lungs of every investigated mouse by electron microscopy (Figure E9). Lipofibroblasts in the lungs of hyperoxic wild-type mice were embedded in a large quantity of elastin, whereas those in the lungs of hyperoxic $p16^{INK4a-/-}$ mice were not surrounded by elastin but were rather associated with thin septa and well-preserved epithelial cells, similar to those of the room-air wild-type mice (Figure E9). Overall, $p16^{INK4a}$ deficiency was associated with the lipogenic differentiation of fibroblasts in the stem cell niche after hyperoxia.

We next used another model of alveolarization, left pneumonectomy, which leads to compensatory neoalveolarization of the remaining lung (Figure 6A) (44–46). Ten days after pneumonectomy, $p16^{INK4a}$ expression in the lung was higher than in that of sham wild-type mice (Figure 6B). The number of lipofibroblasts but also of AT2 cells was higher in the alveolar wall of $p16^{INK4a-/-}$ mice than in wild-type mice (Figures 6C–6F) after surgery, confirming the induction of both cell types by $p16^{INK4a}$ deficiency.

Overall, these results show that $p16^{INK4a}$ may play a major role in lung regeneration and the induction of lipofibroblasts in various models.

$p16^{INK4a}$ Deficiency Induces Early M2 Macrophage Polarization, Which Is Not, However, Involved in Lipofibroblast Differentiation

$p16^{INK4a}$ deficiency has been reported to induce M2 macrophages (47, 48), which could regulate lung regeneration (45, 49–52). We therefore evaluated whether $p16^{INK4a}$ deficiency induces a switch from M1 to M2 macrophages during hyperoxia to trigger lung regeneration through the induction of lipofibroblasts.

Figure 5. (*Continued*). protein), and *Ldlr* (low-density lipoprotein receptor) relative to that of the housekeeping gene *Hprt1* (hypoxanthine-guanine phosphoribosyl transferase 1). (*D*) Wound healing after the scratch assay was significantly faster for $p16^{INK4a-/-}$ fibroblasts than for wild-type (WT) fibroblasts. (*E*) LipidTOX staining in lung. (*F*) Lipid-droplet counts. (*G*) Costaining of pro-SpC (in green) and ADRP (in red). (*H*) Quantification of ADRP at Day 14 (D14) and D60. (*I*) Quantification of pro-SpC at D120. (*J*) Distribution of alveolar type 2 (AT2) lipofibroblasts with mean distance between AT2 cells and lipofibroblasts. (*K*) Flow cytometry showing greater numbers of $CD45^{-}$, $CD31^{-}$, $EpCAM^{-}$ (epithelial cell adhesion molecule–negative), and $PDGFR\alpha^{+}$ (platelet-derived growth factor α-positive) cells and $CD45^{-}$, $CD31^{-}$, $EpCAM^{-}$, $LipidTOX^{+}$, and $ADRP^{+}$ cells at D60 in hyperoxic $p16^{INK4a-/-}$ mice than in WT mice. Scale bars, 20 μm. $^{*}P < 0.05$ and $^{**}P < 0.01$. FITC = fluorescein isothiocyanate; HYX = hyperoxic mice; NOX = normoxic mice; Q = quartile.

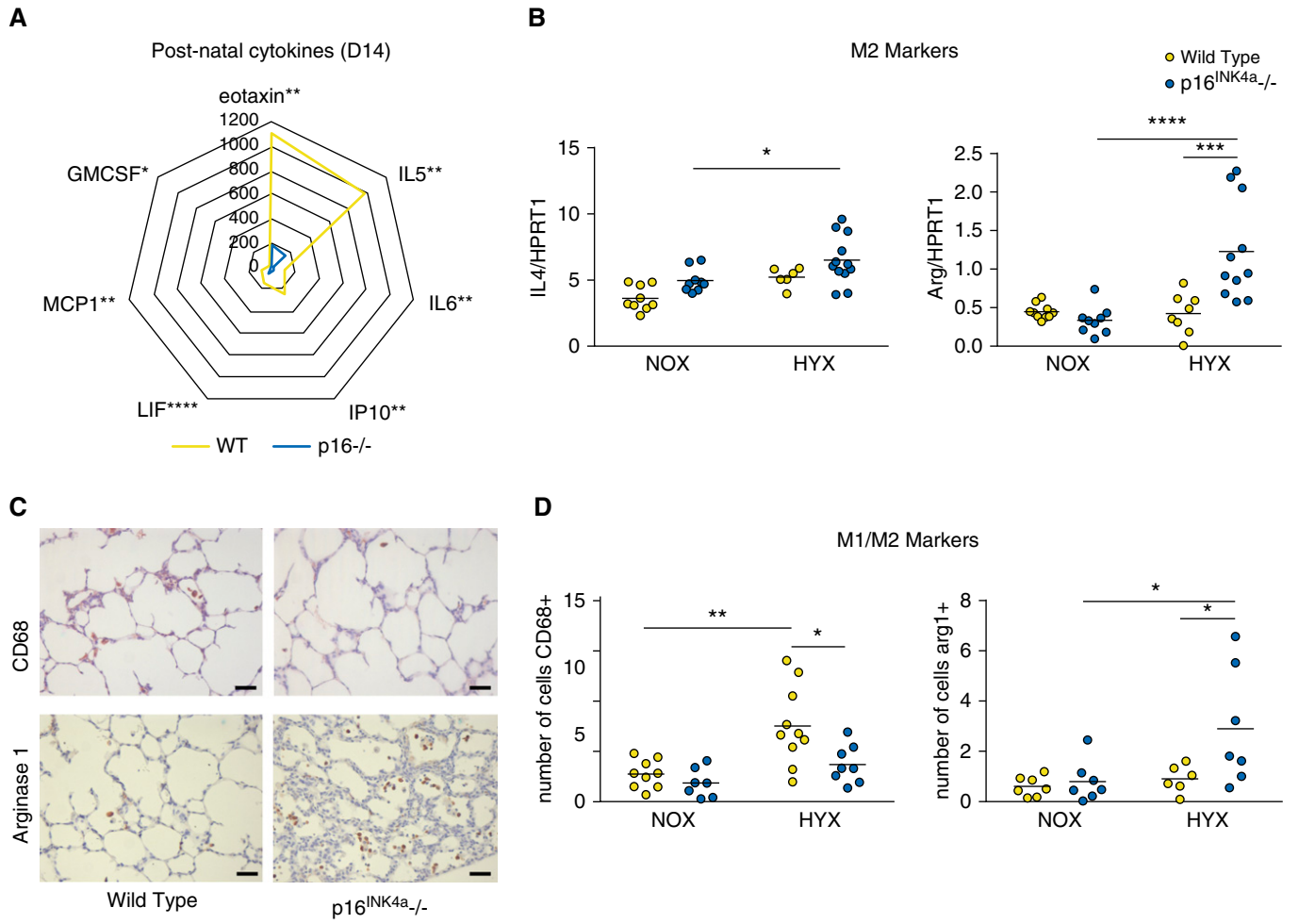

Figure 7. p16^{INK4a} deficiency induces macrophage polarization toward the M2 phenotype and is involved in lipofibroblast differentiation. (*A*) Luminex assay for inflammatory cytokines of whole lung from wild-type (WT) and p16^{INK4a} mice just after hyperoxia. (*B*) PCR of IL4 relative to that of the housekeeping gene HPRT1 (hypoxanthine-guanine phosphoribosyl transferase 1) of whole lung (left) and quantitative PCR of arginase 1 relative to that of the housekeeping gene HPRT1 of whole lung (right). (*C* and *D*) Immunostaining (*C*) and quantification (*D*) of the M1 marker (CD68) and the M2 marker (arginase 1). Yellow circles indicate WT; blue circles indicate p16$^{INK4a-/-}$. Scale bars, 20 μm. *$P < 0.05$, **$P < 0.01$, ***$P < 0.001$, and ****$P < 0.0001$. D14 = Day 14; GMCSF = granulocyte–macrophage colony–stimulating factor; HYX = hyperoxic mice; IP10 = IFN-γ–induced protein 10; LIF = leukemia inhibitory factor; MCP1 = monocyte chemoattractant protein 1; NOX = normoxic mice.

Microarray and Luminex analyses of whole-lung homogenates showed upregulation of inflammatory pathways at D14 in hyperoxic versus normoxic mice. This response was abrogated by p16^{INK4a} deficiency, which was also associated with higher concentrations of IL-4 and arginase 1 (Figures 7A–7D and E8). The results were similar concerning both M1 (CD68) and M2 (arginase 1 and CD163) markers, with higher concentrations of CD68 after hyperoxia in wild-type mice than in p16$^{INK4a-/-}$ mice, whereas arginase 1 and CD163 concentrations changed in opposite directions (Figure 7D). However, M1/M2 modulation by p16^{INK4a} deficiency after hyperoxia was only transient (Figure E8B). These results show that the p16$^{INK4a-/-}$ macrophages underwent early and very short-lasting functional changes, which were temporally dissociated from lipofibroblast activation, making it unlikely that they are responsible for this process.

The Lipogenic Switch of Fibroblasts Can Induce Lung Regeneration after Postnatal Hyperoxia after Lesions Are Established

We further tested the hypothesis that p16^{INK4a} deficiency induces lung regeneration through lipofibroblasts. We first tested whether lipofibroblasts were able to induce a process of alveolar regeneration by using an organoid assay. Lipofibroblasts were isolated as Sca1^{+}LipidTOX^{+} cells and compared with Sca1^{+}LipidTOX^{-} resident stromal cells. They were cocultured with Lyso^{+}Tom^{high} (lysosome-positive and Tom^{high}) AT2 cells (Figure 8A). Organoids did not form with Sca1^{+}LipidTOX^{-} resident stromal cells. The organoids' size ranged from 50 to 350 μm with lipofibroblasts and was associated with a colony-forming efficiency of 5.2. Immunofluorescence staining of organoids for DAPI, Sftpc (AT2-cell marker) and Hopx (AT1-cell marker) indicated that lipofibroblasts support AT2 stem-cell differentiation into AT1 cells (Figures 8B–8D).

We next treated mice with a PPARγ agonist, rosiglitazone, which induces lipofibroblasts (36, 53–55), from just after hyperoxia (D14) until adulthood (D60). In addition, we also assessed the effects of a SREBP activator, T0901317 (Figure 8E), as

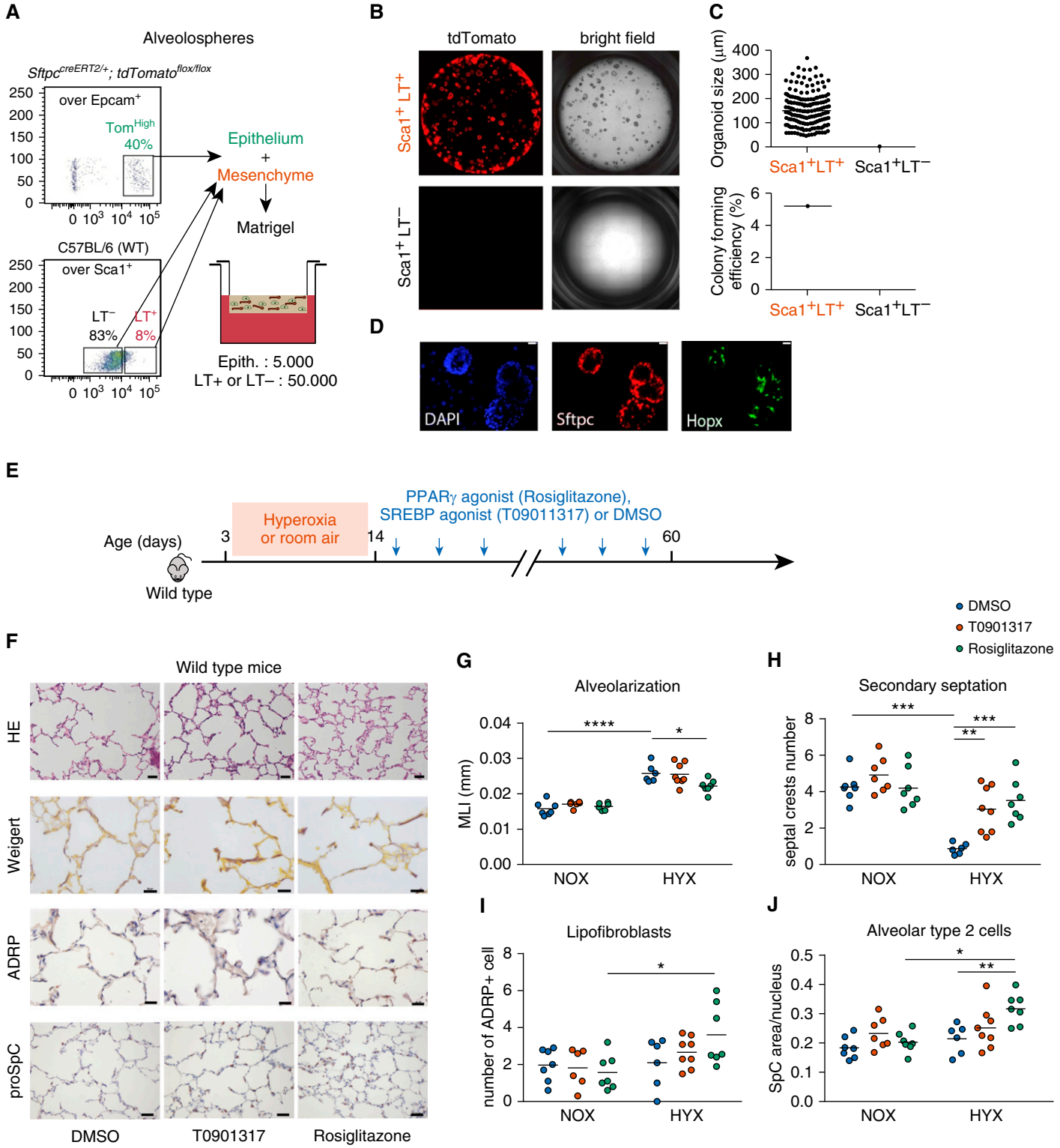

Figure 8. The lipogenic switch of fibroblasts can induce lung regeneration after postnatal hyperoxia. (*A*) Sca1^{+}LT^{+} (spinocerebellar ataxia type 1-positive and LipidTOX^{+}) cells support the self-renewal and differentiation of alveolar type 2 (AT2) stem cells. *Sftpc*$^{CreERT2/+}$; *tdTomato*$^{flox/flox}$ (phenotype with Cre recombinase fused to a mutant estrogen ligand–binding domain *Sftpc* allele variant/wild-type [WT] *Sftpc* allele variant; floxed tandem-dimer Tomato) and C57BL6 (WT) mice 6–8 weeks of age were used to sort Lyso^{+}Tom^{high} (lysosome-positive and translocase of the outer mitochondrial membrane–high) AT2 cells and Sca1^{+}LT^{+} or Sca1^{+}LT$^{−}$ resident stromal cells. Mixture of cells was seeded in Matrigel in 24-well Transwell supports. (*B*) Fluorescence and bright-field picture of representative wells at Day 14. (*C*) Quantification of organoid size (50–350 vs. 0 µm, in Sca1^{+}LT^{+} vs. Sca1^{+}LT$^{−}$, respectively) and colony-forming efficiency (5.2 vs. 0 in Sca1^{+}LT^{+} vs. Sca1^{+}LT$^{−}$, respectively). (*D*) Immunofluorescence staining of organoids for DAPI, Sftpc (AT2 cell marker), and Hopx (AT1 cell marker),

Table 1. Characteristics of Newborns

	Full-Term	Preterm	*P* Value
Subjects, *n*	7	7	—
Gestational age, wk, mean ± SD	40.0 ± 1.4	25.0 ± 0.7	0.0006
Sex, M, *n* (%)	4 (57)	5 (71)	0.99
Weight at birth, g, mean ± SD	3,580 ± 206	770 ± 65	0.0006
Death, *n*	0	2	0.05
Bronchopulmonary dysplasia, *n*	0	2	0.01
Need for noninvasive ventilation at 36 wk of corrected gestational age, *n*	0	2	0.01
Relative $p16^{INK4a}$ expression in cord blood, mean ± SD	0.85 ± 0.81	5.88 ± 11.85	0.0065

the SREBP pathway was highly modulated in the microarray analyses.

Rosiglitazone did not modify lung structure in normoxia-exposed mice, but the MLI and number of septal crests was higher at adulthood than in nontreated mice. This was associated with higher numbers of lipofibroblasts and AT2 cells in the lungs of hyperoxic mice (Figures 8F–8H). SREBP activation increased secondary septation but not the MLI (Figures 8F–8J). Overall, inducing lipofibroblasts through a PPARγ agonist in a curative way was sufficient to induce lung regeneration after hyperoxia-induced hypoalveolarization.

Again, these data show that $p16^{INK4a}$ deficiency promotes the alveolar regeneration process, involving lipogenesis pathways and lipofibroblasts in the stem cell niche.

$p16^{INK4a}$ Concentration Increases in the Blood of Preterm Newborns, Persists in Survivors of BPD, and Is High in the Lungs of Patients with BPD

We assessed $p16^{INK4a}$ concentrations in the blood of six preterm children, born before 24 weeks of gestational age, and six children born at full term, matched for sex and date of birth (56). The subject characteristics are presented in Table 1. $p16^{INK4a}$ concentrations were significantly higher in preterm newborns than in those born at full term (Figure 9A) (57).

We next examined $p16^{INK4a}$ concentrations in the blood of 30 survivors of BPD, who were 7–15 years old, and 27 full-term children without BPD (Table 2). The patients with former BPD (born at a mean gestational age of 28 wk) were mostly male, with a mean age of 8.9 years, and had small alterations of lung function (mean FEV_1 after bronchodilation, 1.37 ± 0.39 L). Interestingly, $p16^{INK4a}$ induction persisted in the blood of survivors of BPD (Figure 9B).

In addition, $p16^{INK4a}$ expression was higher in lungs damaged by BPD than in those of premature infants without BPD (Figures 9C and 9D) (58). Most of the cells in the lungs of patients with BPD expressed $p16^{INK4a}$, especially within interstitial tissue, but not in the alveolar epithelium. Furthermore, data from the LungMAP consortium (lungmap.net) shows nearly no lung expression of this protein before 4 years of age in humans.

Thus, prematurity induces $p16^{INK4a}$ in the blood and lungs, and such overexpression persists in survivors BPD.

Discussion

Here, we show *1*) that $p16^{INK4a}$ deficiency may play a major role in lung regeneration, independently of aging or senescence; *2*) a curative and not only preventive effect of the clearance of $p16^{INK4a}$ cells on lung structure; and *3*) the ability of a PPARγ agonist to induce lung regeneration once lung lesions are established (Figure 9E). We also found that prematurity induced $p16^{INK4a}$ expression in the blood and lungs, which persisted in survivors of BPD. Overall, our results offer new therapeutic perspectives.

Previous studies have shown the accumulation of $p16^{INK4a+}$ cells during aging, providing evidence that $p16^{INK4a}$ may be a driver of the multiorgan age-related phenotype (11, 12, 59–61). Moreover, $p16^{INK4a}$ deletion has been shown to have a regenerative potential after the damaging of slow-turnover tissues, pancreas, and brain (7, 9). However, this effect has only been observed in aged organisms. For example, pancreatic-islet proliferation and diabetes-specific survival were not affected by $p16^{INK4a}$ deficiency in young mice but increased in older $p16^{INK4a-/-}$ mice (7). Interestingly, the clearance of $p16^{INK4a+}$ cells improved pulmonary function without improving lung histology after bleomycin-induced fibrosis in mice (62). In our study, we demonstrate that $p16^{INK4a}$ deficiency drives regeneration, leading to the original organ architecture and not only to partial repair with extracellular matrix accumulation (34). The alveolospheres experiment confirmed that lipofibroblasts are

Figure 8. (*Continued*). indicating that lipofibroblasts ($Sca1^+LT^+$) support AT2 stem cell differentiation into AT1 cells (scale bars, 100 μm). (*E*) Timeline of exposure to hyperoxia. WT mice were exposed to hyperoxia, versus room air, from Day 3 to Day 14 and were then exposed to room air. One group was treated with rosiglitazone (PPARγ [peroxisome proliferator–activated receptor γ] agonist), another group was treated with T0901317 (activator of SREBP [sterol regulatory element–binding protein]), and another group was treated with vehicle from Day 15 to Day 60. Lungs were harvested at Day 60. (*F*) HE staining and elastin staining by the Weigert technique. Immunostaining for ADRP (adipose differentiation–related protein) or pro-SpC was used. Scale bars, 20 μm. (*G*) Quantification of the MLI. (*H*) Septal crest counts. (*I*) Quantification of the area of ADRP staining/nuclear staining. (*J*) Quantification of the area of pro-SpC staining/nuclear staining. Blue circles indicate vehicle; red circles indicate T0901317; green circles indicate rosiglitazone. $^*P < 0.05$, $^{**}P < 0.01$, $^{***}P < 0.001$, and $^{****}P < 0.0001$. Epcam = epithelial cell adhesion molecule; HE = hematoxylin and eosin; HYX = hyperoxic mice; MLI = mean linear intercept; NOX = normoxic mice.

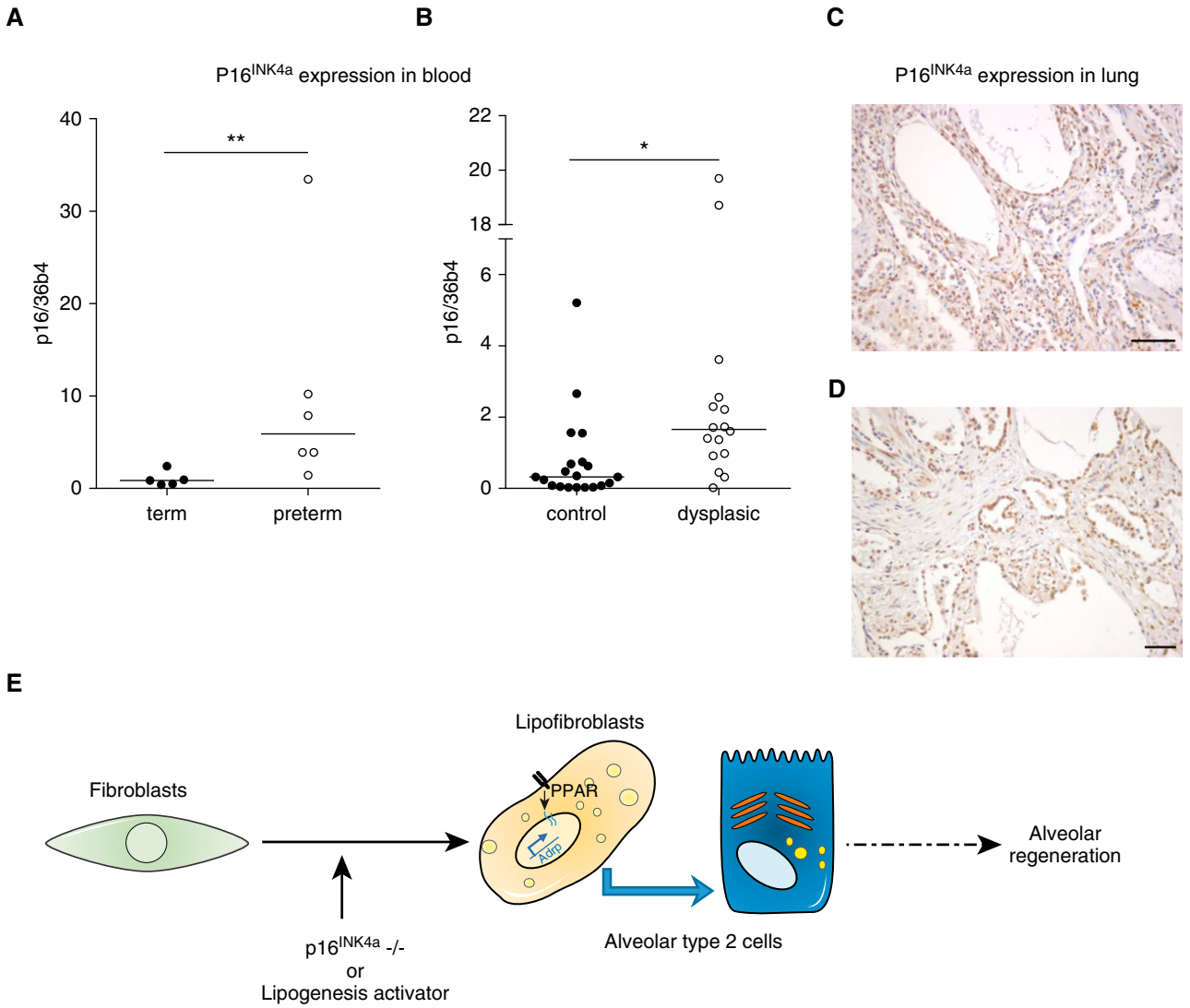

Figure 9. $p16^{INK4a}$ concentrations increase in the blood of preterm newborns, persist in survivors of bronchopulmonary dysplasia (BPD), and are high in the lungs of patients BPD. (*A*) Gene expression by quantitative PCR (qPCR) of $p16^{INK4a}$ relative to that of the housekeeping gene 36B4 (acidic ribosomal phosphoprotein P0) at birth, using peripheral blood mononuclear cells extracted from the cord blood of preterm or full-term newborns. (*B*) Gene expression by qPCR of $p16^{INK4a}$ relative to that of the housekeeping gene 36B4 at 7–15 years old, using peripheral blood mononuclear cells extracted from the peripheral blood of patients with former dysplasia matched to control animals for age and sex. (*C* and *D*) Representative images of $p16^{INK4a}$ expression in the lungs of newborns who died of BPD. Scale bars, 20 μm. (*E*) Schematic diagram showing the switch of fibroblasts to lipofibroblasts, through $p16^{INK4a}$ deletion or the activation of lipogenesis, and its role in alveolar regeneration via alveolar type 2 cells.*$P < 0.05$ and **$P < 0.01$. PPAR = peroxisome proliferator–activated receptor.

specifically able to support AT2 cell growth. The regeneration process evolves through a number of steps, starting with extracellular matrix deposition concomitant with alveolarization, which then disappears, resulting in the healthy restoration of alveolar airspaces. This suggests that an aberrant repair process, which involves fibrosis, was reversed by $p16^{INK4a}$ deficiency during late adulthood (62). Moreover, the proregenerative potential of $p16^{INK4a}$ deficiency was confirmed in the pneumonectomy model, which is free of any initial lung injury.

An important point highlighted by his study is the ability of the clearance of $p16^{INK4a+}$ cells to restore lung architecture in a curative manner. Clearance of $p16^{INK4a+}$ cells delays several manifestations of aging, prevents neuronal diseases, and attenuates post-traumatic osteoarthritis (11, 12, 61). However, the induction of $p16^{INK4a+}$ cell clearance was not initiated once the diseases were established. Here, we treated $p16^{INK4a}$ *ATTAC* mice after D14, once hyperoxia-induced lesions were clearly established. After 45 days of treatment, the lungs of hyperoxia-exposed mice showed the same characteristics as the lungs of nonexposed mice, confirming the curative potential of $p16^{INK4a+}$ cell clearance. As $p16^{INK4a+}$ cells are mainly mesenchymal, their elimination may stop inhibitory signals and allow another population of fibroblasts to emerge and induce regeneration.

Table 2. Characteristics of Children Aged 7–15 Years

	Control	Ex-BPD	*P* Value
Subjects, *n*	27	30	—
Age, yr	10.91 ± 2.80	8.92 ± 4.85	0.04
Sex, M/F, *n* (%)	10 (33)/20 (66)	17 (57)/13 (43)	0.03
Gestational age, wk	39.0 ± 1.4	28.0 ± 2.7	0.0001
FEV_1 before BD, L	—	1.37 ± 0.39	—
FEV_1 before BD, % pred	—	69.6 ± 17.3	—
$p16^{INK4a}$ expression in peripheral blood	0.21 ± 0.56	1.10 ± 2.14	0.003

Definition of abbreviations: % pred = percent predicted; BD = bronchodilation; BPD = bronchopulmonary dysplasia.

The specific regenerative role of $p16^{INK4a}$ in young lungs may be due to its involvement in pathways different from those involved during aging. We particularly identified a role of $p16^{INK4a}$ in regulating lipogenesis in mesenchymal cells. Lipofibroblasts appeared as the main proregenerative cells in $p16^{INK4a-/-}$ lungs after hyperoxia. Their increased number in $p16^{INK4a-/-}$ mice after $p16^{INK4a+}$ cell clearance and their proximity to AT2 cells strongly suggest that they belong to the stem cell niche and that $p16^{INK4a}$ deficiency modulates the AT2 environment in a proregenerative manner (42, 63, 64), confirming the essential role of mesenchymal cells (65). This phenomenon has been documented during lung development (35, 37, 38, 66). It has been recently shown that lipofibroblasts can reduce alveolar fibrosis once this disease is established (36). However, the ability of lipofibroblasts to promote lung regeneration was unknown. The effectiveness of the curative administration of a PPARγ agonist, in the same way as $p16^{INK4a}$ deficiency or $p16^{INK4a+}$ cell clearance, strongly supports a role of lipofibroblasts in lung regeneration.

A critical point that emerges from our results is the mechanism by which $p16^{INK4a}$ controls the lipofibroblast switch. Given the similarity between lipofibroblasts and fat progenitors (67, 68), this lipogenic balance may occur through the control of cell senescence by $p16^{INK4a}$, as this contributes to age-dependent dysfunction of fat progenitors rescued by the clearance of $p16^{INK4a+}$ cells (11, 69). However, at least two arguments run counter to a senescence-mediated process: *1*) $p16^{INK4a}$ deficiency was not associated with a decrease in hyperoxia-induced cell senescence in lungs after hyperoxia and *2*) β-galactosidase activity decreased from childhood to adulthood after hyperoxia in wild-type mice to reach the same amount as that of normoxic mice but was not associated with the restoration of lung architecture. Another possibility is a mechanism mediated by immune cells, such as M2 macrophages (70, 71). However, first, inflammatory changes were short-lived, making them unlikely to be responsible for the late-arising fibroblast lipogenic switch. Moreover, an initial depletion of $p16^{INK4a+}$ cells did not lead to lung restoration at adulthood. Finally, $p16^{INK4a}$ may modulate lipogenic differentiation through the inhibition of CDK4, which can impair adipocyte differentiation through a reduction in PPARγ activity (72).

Overall, this study, including human data in preterm newborns and children with BPD in preclinical models, highlights the fact that targeting $p16^{INK4a}$ and its downstream partners may be a promising approach to promote lung regeneration after injury. More globally, our results support the concept that tissue regeneration may provide a novel strategy and therapeutic window for the correction of early-life diseases. ■

Author disclosures are available with the text of this article at www.atsjournals.org.

Acknowledgment: The authors thank R. Rottier (Department of Pediatric Surgery, Erasmus Medical Center–Sophia Children's Hospital; Department of Cell Biology, Erasmus Medical Center, Rotterdam, the Netherlands) for his gift of lung samples from patients with bronchopulmonary dysplasia. The authors also thank G. Pryhuber from the LungMAP consortium (Division of Neonatology, Department of Pediatrics, University of Rochester Medical Center, Rochester, NY). The authors also thank Xavier Decrouy, Christelle Micheli (Plateforme Imagerie, Institut Mondor pour la Recherche Biomédicale [IMRB]–Institut National de la Santé et de la Recherche Médicale [Inserm] U955, Créteil, France), Sébastien Jacques (Plateforme Séquençage et Génomique, Cochin Institut, Paris, France), Marie Lhomme (Institute of Cardiometabolism and Nutrition, Pitié-Salpêtrière Hospital, Paris, France), Claire Szczepaniak (Microscopie Électronique Centre Imagerie Cellulaire Santé, Clermont-Ferrand, France), and Philippe Caramelle for all animal procedures. The expert technical assistance of M. Surenaud (Luminex plateform, IMRB–Inserm U955, Créteil, France) is also gratefully acknowledged. The assistance of Patrick Ledudal, Amelle Issa, Diane Redel, Mélanie Vassal, Camille Jung (Centre de Recherche Clinique, Ressources du Centre Biologique, Centre Hospitalier Intercommunal de Créteil, France), and Adeline Henry and Aurelie Guguin (Installation de Cytométrie en Flux, IMRB–Inserm U955, Créteil, France) is also sincerely acknowledged. Finally, the authors thank Christophe Delacourt and Arnaud Mailleux for their advice.

References

1. Hogan BL, Barkauskas CE, Chapman HA, Epstein JA, Jain R, Hsia CC, *et al*. Repair and regeneration of the respiratory system: complexity, plasticity, and mechanisms of lung stem cell function. *Cell Stem Cell* 2014;15:123–138.
2. Kotton DN, Morrisey EE. Lung regeneration: mechanisms, applications and emerging stem cell populations. *Nat Med* 2014;20:822–832.
3. Rock JR, Barkauskas CE, Cronce MJ, Xue Y, Harris JR, Liang J, *et al*. Multiple stromal populations contribute to pulmonary fibrosis without evidence for epithelial to mesenchymal transition. *Proc Natl Acad Sci U S A* 2011;108:E1475–E1483.
4. Stolk J, Stockley RA, Stoel BC, Cooper BG, Piitulainen E, Seersholm N, *et al*. Randomised controlled trial for emphysema with a selective agonist of the γ-type retinoic acid receptor. *Eur Respir J* 2012;40:306–312.
5. Roth MD, Connett JE, D'Armiento JM, Foronjy RF, Friedman PJ, Goldin JG, *et al*.; FORTE Study Investigators. Feasibility of retinoids for the treatment of emphysema study. *Chest* 2006;130:1334–1345.
6. Krishnamurthy J, Torrice C, Ramsey MR, Kovalev GI, Al-Regaiey K, Su L, *et al*. Ink4a/Arf expression is a biomarker of aging. *J Clin Invest* 2004; 114:1299–1307.
7. Krishnamurthy J, Ramsey MR, Ligon KL, Torrice C, Koh A, Bonner-Weir S, *et al*. p16INK4a induces an age-dependent decline in islet regenerative potential. *Nature* 2006;443:453–457.

8. Janzen V, Forkert R, Fleming HE, Saito Y, Waring MT, Dombkowski DM, *et al*. Stem-cell ageing modified by the cyclin-dependent kinase inhibitor p16INK4a. *Nature* 2006;443:421–426.
9. Molofsky AV, Slutsky SG, Joseph NM, He S, Pardal R, Krishnamurthy J, *et al*. Increasing p16INK4a expression decreases forebrain progenitors and neurogenesis during ageing. *Nature* 2006;443: 448–452.
10. Baker DJ, Dawlaty MM, Wijshake T, Jeganathan KB, Malureanu L, van Ree JH, *et al*. Increased expression of BubR1 protects against aneuploidy and cancer and extends healthy lifespan. *Nat Cell Biol* 2013;15:96–102.
11. Baker DJ, Childs BG, Durik M, Wijers ME, Sieben CJ, Zhong J, *et al*. Naturally occurring p16(Ink4a)-positive cells shorten healthy lifespan. *Nature* 2016;530:184–189.
12. Baker DJ, Wijshake T, Tchkonia T, LeBrasseur NK, Childs BG, van de Sluis B, *et al*. Clearance of p16Ink4a-positive senescent cells delays ageing-associated disorders. *Nature* 2011;479:232–236.
13. Simpson SJ, Turkovic L, Wilson AC, Verheggen M, Logie KM, Pillow JJ, *et al*. Lung function trajectories throughout childhood in survivors of very preterm birth: a longitudinal cohort study. *Lancet Child Adolesc Health* 2018;2:350–359.
14. Wong PM, Lees AN, Louw J, Lee FY, French N, Gain K, *et al*. Emphysema in young adult survivors of moderate-to-severe bronchopulmonary dysplasia. *Eur Respir J* 2008;32:321–328.
15. Gough A, Linden M, Spence D, Patterson CC, Halliday HL, McGarvey LP. Impaired lung function and health status in adult survivors of bronchopulmonary dysplasia. *Eur Respir J* 2014;43:808–816.
16. Islam JY, Keller RL, Aschner JL, Hartert TV, Moore PE. Understanding the short- and long-term respiratory outcomes of prematurity and bronchopulmonary dysplasia. *Am J Respir Crit Care Med* 2015;192: 134–156.
17. Jobe AH, Abman SH. Bronchopulmonary dysplasia: a continuum of lung disease from the fetus to the adult. *Am J Respir Crit Care Med* 2019;200:659–660.
18. Moschino L, Stocchero M, Filippone M, Carraro S, Baraldi E. Longitudinal assessment of lung function in survivors of bronchopulmonary dysplasia from birth to adulthood: the Padova BPD study. *Am J Respir Crit Care Med* 2018;198:134–137.
19. Narayanan M, Beardsmore CS, Owers-Bradley J, Dogaru CM, Mada M, Ball I, *et al*. Catch-up alveolarization in ex-preterm children: evidence from (3)He magnetic resonance. *Am J Respir Crit Care Med* 2013; 187:1104–1109.
20. Ribeiro Baptista B, Zysman M, Essari LA, Giffard C, Franco-Montoya ML, Epaud R, *et al*. Lipogenic switch of fibroblast to lipofibroblast induce lung regeneration in a model of bronchopulmonary dysplasia [abstract]. *Eur Respir J* 2019;54:PA4119.
21. Ribeiro Baptista B, Zysman M, Souktani R, Giffard C, Lize M, Pons S, *et al*. Increased proliferation of type 2 alveolar epithelial cells in a pneumonectomy model mice with a deletion of p16ink4a gene [abstract]. *Eur Respir J* 2018;52:PA590.
22. Zysman M, Essari LA, Franco-Montoya ML, Vibhushan S, Caramelle P, Souktani R, *et al*. P16 in bronchopulmonary dysplasia: Early determinant of respiratory disease [abstract]? *Eur Respir J* 2017;50: PA4186.
23. Krimpenfort P, Quon KC, Mooi WJ, Loonstra A, Berns A. Loss of p16Ink4a confers susceptibility to metastatic melanoma in mice. *Nature* 2001;413:83–86.
24. Lopez E, Boucherat O, Franco-Montoya ML, Bourbon JR, Delacourt C, Jarreau PH. Nitric oxide donor restores lung growth factor and receptor expression in hyperoxia-exposed rat pups. *Am J Respir Cell Mol Biol* 2006;34:738–745.
25. Lee PJ, Alam J, Sylvester SL, Inamdar N, Otterbein L, Choi AM. Regulation of heme oxygenase-1 expression *in vivo* and *in vitro* in hyperoxic lung injury. *Am J Respir Cell Mol Biol* 1996;14: 556–568.
26. Takahashi Y, Izumi Y, Kohno M, Kimura T, Kawamura M, Okada Y, *et al*. Thyroid transcription factor-1 influences the early phase of compensatory lung growth in adult mice. *Am J Respir Crit Care Med* 2010;181:1397–1406.
27. Burri PH, Dbaly J, Weibel ER. The postnatal growth of the rat lung: I. Morphometry. *Anat Rec* 1974;178:711–730.
28. Kayser BD, Lhomme M, Prifti E, Da Cunha C, Marquet F, Chain F, *et al*. Phosphatidylglycerols are induced by gut dysbiosis and inflammation, and favorably modulate adipose tissue remodeling in obesity. *FASEB J* 2019;33:4741–4754.
29. Kool HM, Bürgisser PE, Edel GG, de Kleer I, Boerema-de Munck A, de Laat I, *et al*. Inhibition of retinoic acid signaling induces aberrant pericyte coverage and differentiation resulting in vascular defects in congenital diaphragmatic hernia. *Am J Physiol Lung Cell Mol Physiol* 2019;317:L317–L331.
30. Tsuji T, Aoshiba K, Nagai A. Alveolar cell senescence in patients with pulmonary emphysema. *Am J Respir Crit Care Med* 2006;174: 886–893.
31. Dagouassat M, Gagliolo JM, Chrusciel S, Bourin MC, Duprez C, Caramelle P, *et al*. The cyclooxygenase-2-prostaglandin E2 pathway maintains senescence of chronic obstructive pulmonary disease fibroblasts. *Am J Respir Crit Care Med* 2013;187:703–714.
32. Amsellem V, Gary-Bobo G, Marcos E, Maitre B, Chaar V, Validire P, *et al*. Telomere dysfunction causes sustained inflammation in chronic obstructive pulmonary disease. *Am J Respir Crit Care Med* 2011; 184:1358–1366.
33. Barnes PJ, Baker J, Donnelly LE. Cellular senescence as a mechanism and target in chronic lung diseases. *Am J Respir Crit Care Med* 2019; 200:556–564.
34. Beers MF, Morrisey EE. The three R's of lung health and disease: repair, remodeling, and regeneration. *J Clin Invest* 2011;121:2065–2073.
35. Al Alam D, El Agha E, Sakurai R, Kheirollahi V, Moiseenko A, Danopoulos S, *et al*. Evidence for the involvement of fibroblast growth factor 10 in lipofibroblast formation during embryonic lung development. *Development* 2015;142:4139–4150.
36. El Agha E, Moiseenko A, Kheirollahi V, De Langhe S, Crnkovic S, Kwapiszewska G, *et al*. Two-way conversion between lipogenic and myogenic fibroblastic phenotypes marks the progression and resolution of lung fibrosis. *Cell Stem Cell* 2017;20:571.
37. Walther TC, Farese RV Jr. Lipid droplets and cellular lipid metabolism. *Annu Rev Biochem* 2012;81:687–714.
38. Tatsumi T, Takayama K, Ishii S, Yamamoto A, Hara T, Minami N, *et al*. Forced lipophagy reveals that lipid droplets are required for early embryonic development in mouse. *Development* 2018;145: dev161893.
39. McGowan SE, McCoy DM. Regulation of fibroblast lipid storage and myofibroblast phenotypes during alveolar septation in mice. *Am J Physiol Lung Cell Mol Physiol* 2014;307:L618–L631.
40. Fu X, Khalil H, Kanisicak O, Boyer JG, Vagnozzi RJ, Maliken BD, *et al*. Specialized fibroblast differentiated states underlie scar formation in the infarcted mouse heart. *J Clin Invest* 2018;128:2127–2143.
41. Li C, Lee MK, Gao F, Webster S, Di H, Duan J, *et al*. Secondary crest myofibroblast PDGFRα controls the elastogenesis pathway via a secondary tier of signaling networks during alveologenesis. *Development* 2019;146:dev176354.
42. Barkauskas CE, Cronce MJ, Rackley CR, Bowie EJ, Keene DR, Stripp BR, *et al*. Type 2 alveolar cells are stem cells in adult lung. *J Clin Invest* 2013;123:3025–3036.
43. Zepp JA, Zacharias WJ, Frank DB, Cavanaugh CA, Zhou S, Morley MP, *et al*. Distinct mesenchymal lineages and niches promote epithelial self-renewal and myofibrogenesis in the lung. *Cell* 2017;170: 1134–1148, e10.
44. Green J, Endale M, Auer H, Perl AK. Diversity of interstitial lung fibroblasts is regulated by platelet-derived growth factor receptor α kinase activity. *Am J Respir Cell Mol Biol* 2016;54:532–545.
45. Lechner AJ, Driver IH, Lee J, Conroy CM, Nagle A, Locksley RM, *et al*. Recruited monocytes and type 2 immunity promote lung regeneration following pneumonectomy. *Cell Stem Cell* 2017;21: 120–134, e7.
46. Chung MI, Bujnis M, Barkauskas CE, Kobayashi Y, Hogan BLM. Niche-mediated BMP/SMAD signaling regulates lung alveolar stem cell proliferation and differentiation. *Development* 2018;145:dev163014.
47. Fuentes L, Wouters K, Hannou SA, Cudejko C, Rigamonti E, Mayi TH, *et al*. Downregulation of the tumour suppressor p16INK4A contributes to the polarisation of human macrophages toward an adipose tissue macrophage (ATM)-like phenotype. *Diabetologia* 2011;54:3150–3156.

48. Cudejko C, Wouters K, Fuentes L, Hannou SA, Paquet C, Bantubungi K, *et al*. p16INK4a deficiency promotes IL-4-induced polarization and inhibits proinflammatory signaling in macrophages. *Blood* 2011; 118:2556–2566.
49. Kalymbetova TV, Selvakumar B, Rodríguez-Castillo JA, Gunjak M, Malainou C, Heindl MR, *et al*. Resident alveolar macrophages are master regulators of arrested alveolarization in experimental bronchopulmonary dysplasia. *J Pathol* 2018;245:153–159.
50. Chamoto K, Gibney BC, Ackermann M, Lee GS, Lin M, Konerding MA, *et al*. Alveolar macrophage dynamics in murine lung regeneration. *J Cell Physiol* 2012;227:3208–3215.
51. Chamoto K, Gibney BC, Lee GS, Ackermann M, Konerding MA, Tsuda A, *et al*. Migration of $CD11b^{+}$ accessory cells during murine lung regeneration. *Stem Cell Res (Amst)* 2013;10:267–277.
52. Wynn TA, Chawla A, Pollard JW. Macrophage biology in development, homeostasis and disease. *Nature* 2013;496:445–455.
53. Milam JE, Keshamouni VG, Phan SH, Hu B, Gangireddy SR, Hogaboam CM, *et al*. PPAR-gamma agonists inhibit profibrotic phenotypes in human lung fibroblasts and bleomycin-induced pulmonary fibrosis. *Am J Physiol Lung Cell Mol Physiol* 2008;294: L891–L901.
54. Rehan VK, Sugano S, Wang Y, Santos J, Romero S, Dasgupta C, *et al*. Evidence for the presence of lipofibroblasts in human lung. *Exp Lung Res* 2006;32:379–393.
55. Dasgupta C, Sakurai R, Wang Y, Guo P, Ambalavanan N, Torday JS, *et al*. Hyperoxia-induced neonatal rat lung injury involves activation of TGF-beta and Wnt signaling and is protected by rosiglitazone. *Am J Physiol Lung Cell Mol Physiol* 2009;296:L1031–L1041.
56. Escribano A, Pastor S, Reula A, Castillo S, Vicente S, Sanz F, *et al*. Accelerated telomere attrition in children and teenagers with α1-antitrypsin deficiency. *Eur Respir J* 2016;48:350–358.
57. Vassallo PF, Simoncini S, Ligi I, Chateau AL, Bachelier R, Robert S, *et al*. Accelerated senescence of cord blood endothelial progenitor cells in premature neonates is driven by SIRT1 decreased expression. *Blood* 2014;123:2116–2126.
58. Chao CM, Moiseenko A, Kosanovic D, Rivetti S, El Agha E, Wilhelm J, *et al*. Impact of Fgf10 deficiency on pulmonary vasculature formation in a mouse model of bronchopulmonary dysplasia. *Hum Mol Genet* 2019;28:1429–1444.
59. Bussian TJ, Aziz A, Meyer CF, Swenson BL, van Deursen JM, Baker DJ. Clearance of senescent glial cells prevents tau-dependent pathology and cognitive decline. *Nature* 2018;562:578–582.
60. Farr JN, Xu M, Weivoda MM, Monroe DG, Fraser DG, Onken JL, *et al*. Targeting cellular senescence prevents age-related bone loss in mice. *Nat Med* 2017;23:1072–1079.
61. Jeon OH, Kim C, Laberge RM, Demaria M, Rathod S, Vasserot AP, *et al*. Local clearance of senescent cells attenuates the development of post-traumatic osteoarthritis and creates a pro-regenerative environment. *Nat Med* 2017;23:775–781.
62. Schafer MJ, White TA, Iijima K, Haak AJ, Ligresti G, Atkinson EJ, *et al*. Cellular senescence mediates fibrotic pulmonary disease. *Nat Commun* 2017;8:14532.
63. Torday J, Hua J, Slavin R. Metabolism and fate of neutral lipids of fetal lung fibroblast origin. *Biochim Biophys Acta* 1995;1254:198–206.
64. Schultz CJ, Torres E, Londos C, Torday JS. Role of adipocyte differentiation-related protein in surfactant phospholipid synthesis by type II cells. *Am J Physiol Lung Cell Mol Physiol* 2002;283:L288–L296.
65. Sucre JMS, Vickers KC, Benjamin JT, Plosa EJ, Jetter CS, Cutrone A, *et al*. Hyperoxia injury in the developing lung is mediated by mesenchymal expression of Wnt5A. *Am J Respir Crit Care Med* 2020;201:1249–1262.
66. El Agha E, Herold S, Al Alam D, Quantius J, MacKenzie B, Carraro G, *et al*. Fgf10-positive cells represent a progenitor cell population during lung development and postnatally. *Development* 2014;141: 296–306.
67. Green H, Kehinde O. An established preadipose cell line and its differentiation in culture: II. Factors affecting the adipose conversion. *Cell* 1975;5:19–27.
68. Kliewer SA, Lenhard JM, Willson TM, Patel I, Morris DC, Lehmann JM. A prostaglandin J2 metabolite binds peroxisome proliferator-activated receptor gamma and promotes adipocyte differentiation. *Cell* 1995;83:813–819.
69. Xu M, Palmer AK, Ding H, Weivoda MM, Pirtskhalava T, White TA, *et al*. Targeting senescent cells enhances adipogenesis and metabolic function in old age. *eLife* 2015;4:e12997.
70. Qiu Y, Nguyen KD, Odegaard JI, Cui X, Tian X, Locksley RM, *et al*. Eosinophils and type 2 cytokine signaling in macrophages orchestrate development of functional beige fat. *Cell* 2014;157:1292–1308.
71. Goh YP, Henderson NC, Heredia JE, Red Eagle A, Odegaard JI, Lehwald N, *et al*. Eosinophils secrete IL-4 to facilitate liver regeneration. *Proc Natl Acad Sci U S A* 2013;110:9914–9919.
72. Abella A, Dubus P, Malumbres M, Rane SG, Kiyokawa H, Sicard A, *et al*. Cdk4 promotes adipogenesis through PPARgamma activation. *Cell Metab* 2005;2:239–249.